energy&fuels

Article

pubs.acs.org/EF

Impact of Inorganically Bound Sulfur on Late Shale Gas Generation

Qingtao Wang,[†,‡] Hong Lu,*[,†] Chenchen Shen,[†,‡] Jinzhong Liu,[†] Ping'an Peng,[†] and Chang Samuel Hsu*[,§,∥,⊥]

[†]State Key Laboratory of Organic Geochemistry, Guangzhou Institute of Geochemistry, Chinese Academy of Sciences, Guangzhou 510640, China

[‡]University of Chinese Academic of Sciences, Beijing 100049, China

[§]Department of Chemical and Biomedical Engineering, Florida A&M University/Florida State University, Tallahassee, Florida 32310, United States

[∥]State Key Laboratory of Heavy Oil Processing, China University of Petroleum, Beijing, 102249 China

[⊥]Petro Bio Oil Consulting, Tallahassee, Florida 32312, United States

Supporting Information

ABSTRACT: Nonisothermal, confined pyrolysis was applied to a mature shale sample from the Ordovician Salgan Formation in Tarim Basin, northwest China. Experiments were conducted using gold-tubes with added water at a very slow heating rate (2 °C/h) and end temperatures between 336 and 600 °C. To investigate the influence of inorganically bound sulfur on the generation of gases and to consider the geological occurrence of sulfur-containing minerals, such as prevalent pyrite in shales, the experiments were carried out with and without admixtures of $MgSO_4$, $CaSO_4$, and pyrite. High amounts of methane along with lower amounts of wet gases were formed from highly mature shale without minerals added, demonstrating a huge late gas generation potential at post peak-oil window maturities. In the experiments with added sulfates and pyrite, all organic gases were consumed in varying proportions, resulting in different chemical and stable carbon isotopic compositions. Pyrite treatment affects wet gas (C_2–C_5) evolution directly, but it affects methane (C_1) evolution indirectly. In contrast, sulfate treatments affect C_1–C_5 evolution directly. The cumulative yield ratio of CO_2/H_2S indicates that pyrite impacts on the hydrocarbon gas generation through low valence sulfur such as S^0 or others, which are associated with H_2S generation. In the pyrite series, the smooth increase in ethane yield at temperatures exceeding 504 °C, together with a concomitant stable carbon isotope reversal, demonstrates a new origin for ethane at high temperatures. The isotopic reversal may come from reactions between water and solid kerogen/coke/pyrobitumen. Isotopic reversal of ethane occurs only in the control and pyrite series but not in the sulfate treatments. This provides evidence that anoxic conditions are required. Thus, one can expect to encounter isotopic reversals in high maturity, unconventional gas shale environments in the presence of pyrite.

1. INTRODUCTION

According to the classical hydrocarbon generation theory,[1] the main products of liquid petroleum are derived from thermal cracking of kerogen in the low maturity range between 0.5 and 1.3% vitrinite reflectance (νRo), while gasoline range alkanes are predominantly generated at higher thermal maturities (νRo > 1.3%). The recent success in shale gas production, mainly in the maturity range 1.2–1.6% (νRo),[2] attracts more attention to gas generation at even higher maturities. Related experiments demonstrate that late gas generation might come from the cracking of a stable moiety previously formed via recombination reactions between liquid hydrocarbons and kerogen.[3] The late gas precursor structures are thought to be associated with terrestrially influenced, aromatic marine organic matter types,[4] which may be phenolic or very heterogeneous.

Organic–inorganic interactions have been studied for years. The most prominent abiotic oxidation of hydrocarbons at high temperatures is thermochemical sulfate reduction (TSR). Some case studies illustrated that branched and normal alkanes in the gasoline range can be easily oxidized.[5−13] Strong TSR even results in the near complete destruction of hydrocarbons.[14,15] As the most stable hydrocarbon gas, methane was believed not to participate in TSR.[16] However, in a case study of southwestern China, a positive relationship between $\delta^{13}C_1$ and gas sourness ($H_2S/(H_2S+C_nH_{2n+2})$) was found,[8] implying the involvement of methane in TSR. In general, calcareous black shale associated with sulfates (e.g., $CaSO_4$) is deposited under transitional, saline-to-hypersaline evaporitic environments.[17] Thus, TSR can occur in the vicinity of shales. On the other hand, pyrite framboids have been widely reported within North American shales,[18,19] revealing the existence of an oxygen depleted sediment interface during depositional times. In hydroliquefaction of oil shale, pyrite was treated as catalyst and thought to promote the production of hydrocarbon gases.[20] Additionally, a linear relationship between pyrite and total organic carbon (TOC) was proposed within the Triassic Doig Formation in Northeast British Columbia.[21] These previous studies imply that pyrite and TOC content are positively correlated having an effect on hydrocarbon generation processes. Isotope rollover (i.e., decrease in $\delta^{13}C$ values with increasing maturity or temperature) becomes a hot topic in the gas industry because it commonly appears at low wetness values

Received: July 29, 2013
Revised: January 10, 2014
Published: January 15, 2014

   dx.doi.org/10.1021/ef401468w | Energy Fuels 2014, 28, 785–793

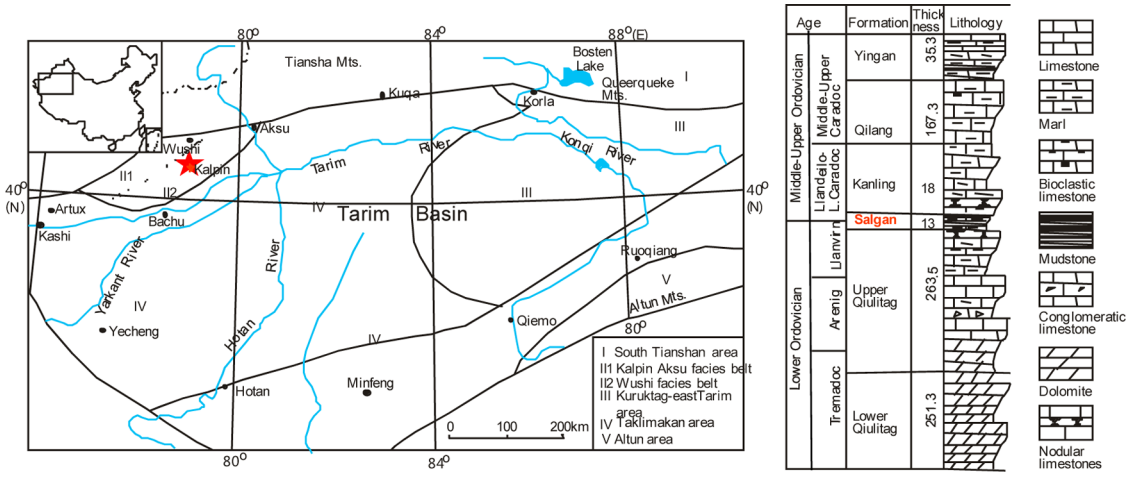

Figure 1. Map of Kalpin (Keping) Valley and stratigraphy in Tarim Basin, Northwest China.

Table 1. Geochemical Data of Ordovician Salgan Shale in Tarim Basin, Northwestern China[a]

sample	age	$\delta^{13}C_{-org}$ (‰)	νRo (%)	TOC (%)	T_{max} (°C)	S_1 (mg/g rock)	S_2 (mg/g rock)	S_3 (mg/g rock)	HI	OI	S (%)
Salgan shale	O_{2-3}	−30.5	1.36	2.27	449	0.57	2.6	0.18	115	7	0.85

[a] $\delta^{13}C_{org}$, ratio of stable $^{13}C/^{12}C$ isotopes of organic matter with respect to that of the Pee Dee Belemnite (PDB) standard; νRo, vitrinite reflectance (based on the reflectance values of vitrinite-like macerals (νLRo) measured on polished resin-embedded whole rock blocks with a Leica MPV3 photomicroscope,[25] using the empirical equation:[26] $\nu Ro = 0.533 \times \nu LRo + 0.667$); TOC, total organic carbon; S_1, free hydrocarbons; S_2, pyrolyzable hydrocarbons; S_3, CO_2 from organic sources; HI, hydrogen index measured and calculated by Rock-Eval 6; OI, oxygen index measured and calculated by Rock-Eval 6 (standard); S (%), the sulfur content measured by Elementar Vario EL III.

with large shale gas production.[22] This paper reports the impact of pyrite and sulfates on isotope rollover, if it occurs.

We designed a series of closed-system pyrolysis gold-tube experiments using a highly mature shale sample and sulfur-containing minerals to investigate the impact of inorganically bound sulfur on gas generation at high thermal pressure conditions. Water was added in the experiments because it probably is present, to some extent, in real systems. Water would facilitate reactions not available in dry environments, and it may contribute hydrogen and oxygen for the formation of hydrocarbons and oxygenated products.[23] Under the pyrolysis temperatures and pressures used in these experiments, water is present in its supercritical state (>374 °C), a state which is highly unlikely to occur in active petroleum systems. However, the natural system could not be simulated any better in laboratory at much higher temperatures than that in source rocks and reservoirs. Additionally, the added water might be necessary for TSR to occur. Our studies attempt to answer the following questions:

(1) How much gases can be produced from mature shales under different thermal conditions? This question is directly related to the reserves of shale gas and might be answered by control experiments without added minerals.
(2) What is the effect of TSR on gas generation and alteration at high temperatures under conditions which produce no additional liquid hydrocarbons? How does TSR alter the chemical and stable carbon isotopic compositions of C_1−C_5 hydrocarbons, especially for methane and ethane, which are generally dominant in shale gas?
(3) What is the effect of pyrite on gas generation at high thermal pressure, and how does this effect contribute to the production of H_2S?

2. EXPERIMENTAL SECTION

2.1. Reactants. A sample of highly mature shale was collected from outcrops of the Middle and Upper Ordovician Salgan Formation in the Kalpin (Keping) Valley of Tarim Basin, northwest China (Figure 1).[24] The geochemical data of Salgan Shale are listed in Table 1. To exclude inorganic CO_2 being formed during the experimental procedures, carbonate in the sample was removed by HCl digestion. The mineral content of Salgan Shale was determined using XRD analysis. It was found to be composed of quartz (29.7%), feldspar (14.7%), illite (31.9%), and montmorillonite (23.7%), whereas no sulfates were detected.

The minerals $MgSO_4 \cdot 7H_2O$ (≥99%) and $CaSO_4 \cdot 2H_2O$ (≥99%) were purchased from Sigma-Aldrich Fluka Company for TSR studies. Pyrite is a naturally occurring mineral and as such purchased from Alfa Aesar Company.

100−200 mg of sample material was loaded into the gold tubes according to the predetermined quantities of sample (shale) and minerals listed in Table 2. For example, the quantities (expressed by weight, volume, and mole) of sample/H_2O/sulfur minerals are 200 mg/50 μL/0.15 mmol in the first set of experiment. The same quantities of sulfur minerals ($MgSO_4$, $CaSO_4$, and FeS_2) by pairs were added to compare the influence of temperature on gas generation. A control series was also carried out (i.e., using only shale and water without added minerals) to unravel changes induced by sulfates or pyrite.

2.2. Gold-Tube Reactor. Following the approach of reference 35, prior to sample loading empty gold tubes (60 mm × 4.5 mm × 0.25 mm internal diameter) with one end sealed were heated at 800 °C in a muffle furnace for 1 h to remove any residual organic materials. The sample mixtures were then loaded into the gold tubes; the tubes were flushed with inert argon to remove air. The open end of the tubes was crimped and welded under a flow of argon while the other end was submerged in cold water in order to trap any volatiles generated during welding. All tubes were accurately weighed before and after pyrolysis to confirm the structural integrity of the pyrolyzed tubes.[11]

2.3. Non-isothermal Temperature Program. The tubes were heated in a furnace equipped with 12 separate autoclaves maintained at a constant pressure of 50 MPa to prevent them from explosion related to gas generation and consequent pressure build-up. A detailed description of this procedure can be found elsewhere.[27] The experiments were conducted at a very slow heating rate of 2 °C/h and the 12 tubes were separately heated from an initial temperature at 250 °C to one of the following end temperatures: 336, 360, 384, 408, 432, 456, 480, 504, 528, 552, 576, and 600 °C. Consequently, 600 °C was reached after more

dx.doi.org/10.1021/ef401468w | Energy Fuels 2014, 28, 785−793

Table 2. Weights of Shale, Water, and Minerals Used in Simulation Experiments

	shales	control	$MgSO_4$		$CaSO_4$		pyrite	
T (°C)	(mg)	H_2O (mg)	H_2O (mg)	$MgSO_4{\cdot}7H_2O$ (mg)	H_2O (mg)	$CaSO_4{\cdot}2H_2O$ (mg)	H_2O (mg)	FeS_2 (mg)
336	200	50	31.1	36.9	44.6	25.8	50	18
360	200	50	31.1	36.9	44.6	25.8	50	18
384	180	45	26.1	33.21	39.6	23.22	45	16.2
408	180	45	26.1	33.21	39.6	23.22	45	16.2
432	160	40	21.1	29.52	34.6	20.64	40	14.4
456	160	40	21.1	29.52	34.6	20.64	40	14.4
480	140	35	16.1	25.83	29.6	18.06	35	12.6
504	140	35	16.1	25.83	29.6	18.06	35	12.6
528	120	30	11.1	22.14	24.6	15.48	30	10.8
552	120	30	11.1	22.14	24.6	15.48	30	10.8
576	100	25	6.1	18.45	19.6	12.9	25	9
600	100	25	6.1	18.45	19.6	12.9	25	9

than 8 days. The heated tubes were immediately removed and quenched once the respective end temperature was reached.

2.4. GC Analysis of Gas Products and Liquid Hydrocarbons. An auxiliary instrument was used to release the gas from the gold tubes into a gas chromatography (GC) instrument for analyses.[11,27] The auxiliary instrument consists of glass tubes, three outlets, and two valves. The first outlet is connected to a vacuum pump, and the second outlet is connected to a removable lid, through which the gold tube can be inserted into the instrument. The third outlet is connected to the GC instrument. After the whole system was evacuated, the outlet to the vacuum pump was closed via the valve switchover. The gold tube was then pierced and the generated gas filled the space inside the instrument. After reaching equilibrium for ~2 min, the gas mixture was injected into the GC instrument. A more detailed description of the instrument setup can be found in Pan et al.[27]

GC analysis was conducted using a Hewlett−Packard 6890GC, which was custom-configured (Wassen ECE) for simultaneous detection of organic ($\leq C_5$) and inorganic (H_2S, CO_2, H_2) gases. This modified GC instrument (Figure 2) is equipped with eight columns, listed in Table 3,

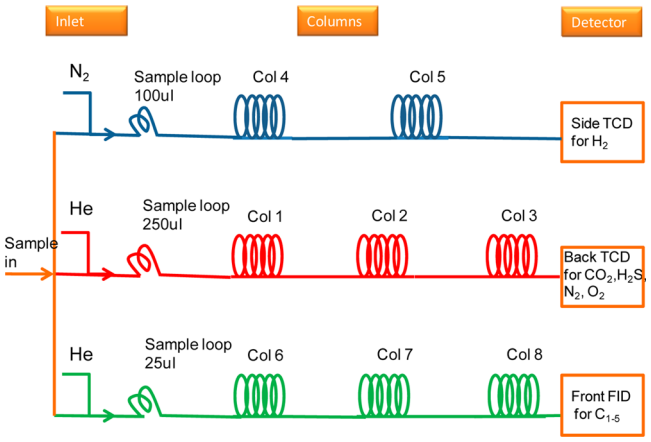

Figure 2. Arrangements of columns and detectors for GC analysis.

and three detectors. A thermal conductivity detector (TCD) was used for analyzing only H_2 (nitrogen as a carrier gas), and another TCD was used for analyzing other inorganic gases (helium as a carrier gas). A flame ionization detector (FID) was used for analyzing gaseous hydrocarbons (helium as a carrier gas). The GC oven was held at 70 °C for 5 min, temperature programmed to 130 °C at 15 °C/min, then to 180 °C at 25 °C/min and held at 180 °C for 4 min.

Figure 3 shows a typical result of the 8-columns/3-detectors GC system for measuring inorganic (CO_2 and H_2S) and organic (C_1−C_5) gases. The top trace shows the hydrogen peak detected by the side TCD, the middle trace shows other inorganic gases, including CO_2, H_2S, O_2, and N_2 determined by the back TCD. The bottom trace shows the organic gases C_1−C_5 measured by the front FID.

Table 3. Columns Used in the Custom-Made Agilent Gas Chromatographic System

column no.	Agilent GC column used
1	0.5m Haysep Q 80/100 mesh
2	6 ft Hayesep Q 80/100 mesh
3	6 ft Molecular Sieve 5A 60/80 mesh
4	3 ft Hayesep Q 80/100 mesh
5	8 ft Molecular Sieve 5A 60/80 mesh
6	2 m × 0.32 mm × 5 μm DB-1 (cut)
7	25 m × 0.32 mm × 8 μm HP-AL/S (GS-Alumina)
8	0.5 m × 0.32 mm × 5 μm DB-1 (cut)

The procedure used to analyze and quantify the liquid hydrocarbon products (C_{6+}) has been reported elsewhere.[27] Briefly, the tubes from the above GC experiment were immersed in liquid nitrogen for cooling for 5 min, then cut swiftly into several pieces in pentane (3 mL in a vial which was subsequently capped) and subjected to 5-min ultrasonic treatments for 5 times and then left to stand for 72 h. A known amount of deuterated n-C_{22} was added as an internal standard for the quantification of C_6+ hydrocarbons (C_6+ yield) using a HP6890 GC.

2.5. Gas Chromatography-Isotope Ratio Mass Spectrometric (GC-irMS) Analysis for Stable Carbon Isotopes. Stable carbon isotope analysis for inorganic gas and gaseous hydrocarbons was conducted on the gas released from the pierced tubes of the above GC experiment, which had been captured in a valve-sealed syringe and injected into a HP 5890 GC interfaced with a VG Isochrom II mass spectrometer. The GC was equipped with a Poraplot Q column (30 m × 0.32 mm i.d.), and helium was used as a carrier gas. The oven was held at 50 °C for 4 min; then, the temperature was ramped to 190 °C at 20 °C/min and held at 190 °C for 5 min. No carbon isotopic measurement was performed for C_6+ hydrocarbons.

3. RESULTS

3.1. Gas Yields. As mentioned, the organic (C_1−C_5) and inorganic (CO_2 and H_2S) gases were measured by gas chromatography. Cumulative gas yields for the different pyrolysis end temperatures are shown in Figure 4.

3.1.1. C_1 Yields (Figure 4a). In the control series, the cumulative methane yield increases over the whole pyrolysis temperature range and reaches a maximum value of 593 μmol/g at 600 °C. The methane yield for the FeS_2 (pyrite) series also exhibits a continuous increase up to 480 °C, resembling that of the control group. Beyond 480 °C, the methane yield reaches a plateau and then increases again for temperatures higher than 528 °C. The methane yield in the $CaSO_4$ series increases up to 480 °C but decreases remarkably at higher thermal stress levels reaching a zero yield at 552 °C. Using $MgSO_4$ as a mineral

dx.doi.org/10.1021/ef401468w | Energy Fuels 2014, 28, 785−793

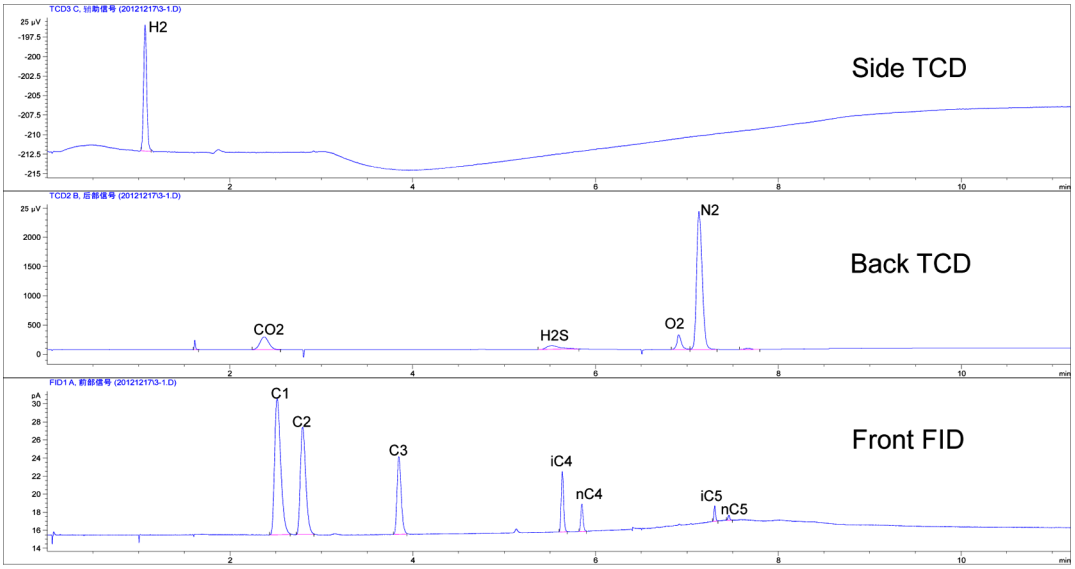

Figure 3. Typical GC outputs from 3 detectors for measuring inorganic and organic gas species.

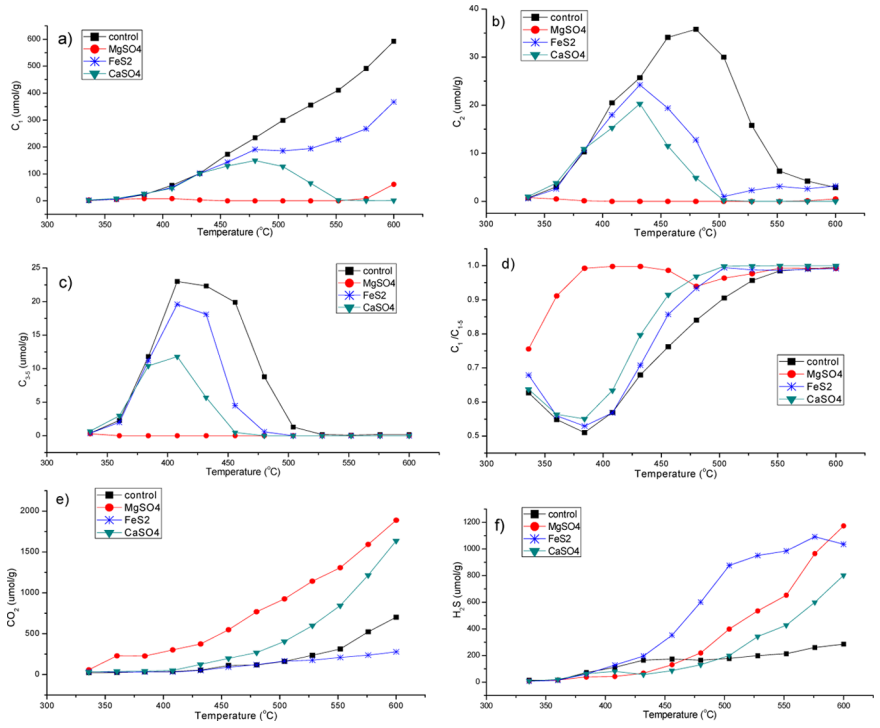

Figure 4. Yields of organic (C_1, C_2, C_3–C_5) and inorganic (CO_2 and H_2S) gases and $C_1/\sum C_{1-5}$ ratio.

admixture, methane yields are negligible from the beginning. Only at highest temperatures methane is formed and stays stable. (see Supporting Information). The highest accumulated yield is detected at the highest experimental temperature (600 °C).

3.1.2. C_2 Yields (Figure 4b). The cumulative yields of ethane reach a maximum value of 36 μmol/g at 480 °C in the control series. In the pyrite and $CaSO_4$ series, maximum yields are detected at a lower temperature of 432 °C and range around 24 μmol/g. In the $MgSO_4$ series ethane is completely consumed over the entire pyrolysis temperature range. Interestingly, ethane yields in the pyrite series reach values almost as low as 0 μmol/g at 504 °C but subsequently gradually increase again with increasing temperatures.

3.1.3. C_3–C_5 Yields (Figure 4c). Since the individual yields of propane, butane, and pentane are very low, they are summed up as C_3–C_5 yields whose evolution with temperature resembles that of ethane, but with lower values and peak temperatures. For the control, pyrite and $CaSO_4$ series maximum cumulative C_3–C_5 yields are observed at 408 °C whereas in the $MgSO_4$ experiments no C_3–C_5 is detected over the entire pyrolysis temperature range again. The profiles of C_1–C_5 in Figure 4a–c confirm a previously proposed viewpoint[28,29] that C_2+ gaseous hydrocarbons are much easier to consume than methane.

3.1.4. $C_1/\sum C_{1-5}$ Ratio (Figure 4d). The gas dryness $C_1/\sum C_{1-5}$ (v/v) in the control, pyrite, and $CaSO_4$ series exhibits a similar evolution with increasing temperature, that is, an initial decrease up to 384 °C and then a gradual increase to 1.0 for

dx.doi.org/10.1021/ef401468w | *Energy Fuels* 2014, 28, 785–793

temperatures between 384 and 600 °C. The initial decrease in $C_1/\sum C_{1-5}$ values below 384 °C is probably due to a more pronounced C_2-C_5 than C_1 production at lower temperatures.[30,31] Above 384 °C, secondary methane formed from the cracking of C_{2+} compounds contributes to the gradual increase of the gas dryness up to maximum temperatures. However, the more rapid increase of gas dryness in the pyrite and $CaSO_4$ cases, for which a value of 1 is reached earlier at ~500 °C, hints to a preferential consumption of wet gases over methane[29−31] either by oxidation or thermal cracking. In contrast, the gas dryness in the $MgSO_4$ series increases to 1.0 rapidly (between 336 °C and 384 °C), which is attributed to the almost complete oxidation of C_{2+} hydrocarbons at very low pyrolysis temperatures (Figure 4b and c).

3.1.5. CO_2 Yields (Figure 4e). The CO_2 yields in all four series increase with pyrolysis temperature, showing highest values in the $MgSO_4$ series, moderate values in the $CaSO_4$ series, and lowest values in the control and pyrite series. High concentrations of CO_2 in the sulfate series should be a result of thermochemical sulfate reduction (TSR) via oxidation of hydrocarbons.[5−8] The amounts of CO_2 produced in the pyrite series were similar to those of the control series at low temperatures but slightly lower above 504 °C.

3.1.6. H_2S Yields (Figure 4f). The H_2S yields in all experiments increase with increasing temperature. The control and pyrite series exhibit similar as well as highest H_2S values up to temperatures of 432 °C. Above 504 °C, the highest and lowest yields of H_2S appear in the control and pyrite series, respectively. The curves of the control and pyrite series do not diverge until 432 °C, indicating that pyrite has its greatest impact on H_2S yield mostly at high temperatures. It can be concluded that generation of H_2S up to 432 °C is mainly related to organically bound sulfur and that reactions involving pyrite become only relevant at temperatures exceeding 432 °C. Meanwhile, intermediate H_2S values can be observed in the two sulfates series. Continuous increase in H_2S yield in the sulfates series can be explained by TSR again.[11,14,16,32] The strong TSR in the $MgSO_4$ series will lead to large amount H_2S. However, the H_2S yield in sulfates series is lower than that in the control series below 456 °C. This might be largely explained by the formation of sulfur-rich pyrobitumen (or pyrobitumen-intermediate). The detection of higher H_2S and much lower CO_2 yields in the experiments involving pyrite compared to those involving sulfates can be attributed to completely different reaction mechanisms, which lead to the alteration of hydrocarbons.

3.1.7. C_{6+} Yields (Liquid Hydrocarbon Yields, Figure 5). In addition to gas yields, liquid yields were studied. The evolution of liquid hydrocarbons with temperature resembles that of C_3-C_5. For the control series, maximum cumulative C_{6+} yields (3.08 mg/g rock) are reached at 456 °C, while the maximum cumulative yields for the pyrite and the $CaSO_4$ series are reached at lower temperatures with lower values, 2.6 mg/g rock at 408 °C and 1.57 mg/g rock at 384 °C, respectively. In the $MgSO_4$ treatment, only trace amounts of liquid hydrocarbons (C_{6+}) are detected over the entire pyrolysis temperature range.

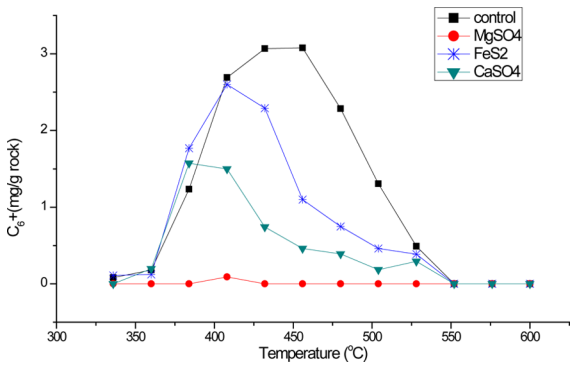

Figure 5. Yields of liquid hydrocarbons (C_{6+}).

3.2. Stable Carbon Isotopes of Organic Gases. The stable carbon isotopic compositions of C_1-C_3 gases and CO_2 are shown in Figure 6. The yields of C_4-C_5 in all experiments and of ethane and propane in the $MgSO_4$ experiments are too low and isotopic compositions could not be determined. Hence, values are not shown in the figures.

As it can be seen in Figure 6a−c, the overall evolutionary trend of $\delta^{13}C$ for C_1-C_3 compounds is the enrichment of ^{13}C with increasing temperature, which can be largely explained by the kinetic isotope effect (KIE). This effect mainly demonstrate the preferential cracking of ^{12}C instead of ^{13}C bonds.[33] Nevertheless, the presence of sulfates and pyrite does affect the KIE, as will be discussed later.

3.2.1. $\delta^{13}C$ of Methane (Figure 6a). Roughly similar $\delta^{13}C$ values for methane were obtained in the control, pyrite, and $CaSO_4$ series, whereas from 480 °C onward $\delta^{13}C$ values for the pyrite and $CaSO_4$ series are slightly but systematically less negative. A remarkable enrichment of ^{13}C occurs for $CaSO_4$ above 504 °C. On the other hand, the $\delta^{13}C$ values of methane in the $MgSO_4$ series are much higher than those in the control series below 480 °C. This phenomenon can be explained by strong oxidation during TSR, which is shown to alter $\delta^{13}C$ composition of gaseous hydrocarbons to a great extent.[6,8,34−36]

3.2.2. $\delta^{13}C$ of Ethane (Figure 6b). No stable carbon isotopic data was obtained for ethane and propane in the $MgSO_4$ series due to insufficient amounts of gas for near complete consumption. The $\delta^{13}C$ evolution of ethane with increasing temperature in the control, pyrite, and $CaSO_4$ series shows an overall increase up to 480 °C. From 480 to 504 °C, more rapid enrichment of ^{13}C occurs in the pyrite and $CaSO_4$ series than in the control series. However, the $\delta^{13}C$ values of ethane in the pyrite series decrease sharply above 504 °C and exhibit values even below those in the control series. The TSR process usually leads to higher $\delta^{13}C$ values of C_2-C_5 due to the preferential consumption of ^{12}C hydrocarbons,[11,34,35] which explains the continuous increase in $\delta^{13}C$ values of ethane in the $CaSO_4$ series. Depleted $\delta^{13}C$ values of ethane in the pyrite series above 504 °C correspond to the gradual increase in ethane yield above 504 °C (Figures 4b and 6b). This indicates that ethane with a lighter isotopic signature is generated at high temperatures from a different precursor structure. As it can be seen in Figures 4c and 5, C_{3+} hydrocarbons have been almost completely consumed at 504 °C. Thus, this "new" ethane cannot be derived from wet gas and C_{6+} liquid hydrocarbons. With water being added in the experiments as a hydrogen source, the reactions between water and solid carbon (coke/kerogen/pyrobitumen) may produce gaseous hydrocarbons such as ethane.

3.2.3. $\delta^{13}C$ of Propane (Figure 6c). The $\delta^{13}C$ compositions of propane in the control, pyrite, and $CaSO_4$ series increase with increasing temperature. For temperatures exceeding 408 °C, the $\delta^{13}C$ values of propane become heavier at a faster rate in the $CaSO_4$ series and than in the pyrite series. Based on Figures 4a−c and 6a−c, it can be seen that C_2+ gaseous hydrocarbons become enriched in ^{13}C once their cumulative yields start to decline. Similar trends were also reported in other laboratories. The enrichment of heavy isotopes of ethane and propane are usually

dx.doi.org/10.1021/ef401468w | Energy Fuels 2014, 28, 785−793

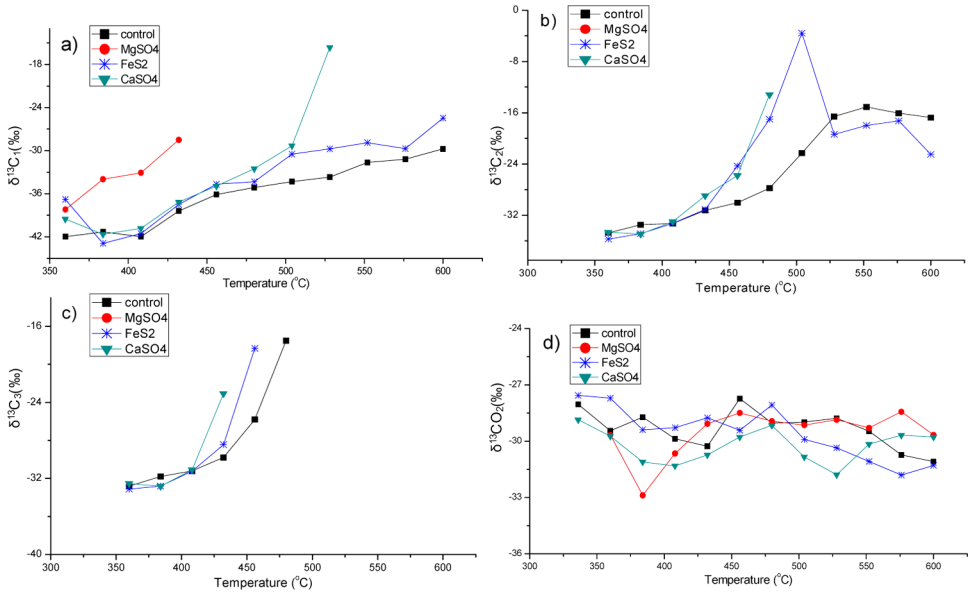

Figure 6. Evolution of stable carbon isotope $\delta^{13}C$ values of methane, ethane, propane, and CO_2 as a function of temperature.

attributed to the KIE, that is, the preferential cracking of $^{12}C-^{12}C$ bonds.[28,37] Here, the higher concentrations of ^{13}C in C_1-C_3 (above 480 °C, 432 °C, 408 °C, respectively) can be additionally ascribed to reactions of minerals (pyrite and $CaSO_4$) with gaseous hydrocarbons, which lead to an enrichment of more $^{13}C-^{13}C$ bonds in the residual gaseous hydrocarbons.

3.2.4. $\delta^{13}C$ of CO_2 (Figure 6d). The stable carbon isotope values of CO_2 fluctuate between −27‰ and −33‰. No systematic or obvious relationships with temperature were found.

4. DISCUSSIONS

4.1. Variations of C_1-C_3 in the Control Series. The generation of gaseous and liquid hydrocarbons need to be collectively considered, because the liquid hydrocarbons can further crack into gases and pyrobitumen at higher thermal pressures.[30,31] However, in the control series, the amounts of generated liquid hydrocarbons (C_{6+}) are very low compared to gaseous hydrocarbons (Figure 4 and 5). Thus, the contribution of secondary gas from C_{6+} cracking to the overall C_1-C_5 gas yield might be limited. Consequently, the yields of gaseous hydrocarbons can be ascribed to the primary cracking of higher molecular weight (MW) analogues in kerogen rather than in oil. On the other hand, wet gas yields can decrease due to their own cracking at high temperatures, because heavier gaseous hydrocarbons are more susceptible to thermal pressure than lighter ones. As a result, the peak yield temperatures in the control series follow the order C_{3-5} (408 °C) < C_2 (480 °C) < C_1 (peak yield for methane is at 600 °C). Methane yields increase with pyrolysis temperature to a maximum value of 593 μmol/g at 600 °C. A further continuous increase of methane yields at temperatures exceeding 600 °C cannot be ruled out. Various sources for late generation, such as kerogen cracking, secondary oil cracking (not in this study), wet gas cracking, decomposition of alkylaromatics at very high temperatures, etc., may provide some theoretical supports for the large yields of methane.[3,4,30,31,33] Our results in the control series imply the existence of a large late gas potential of methane as a resource from mature shales under high thermal pressures.

4.2. Variations of C_1-C_3 in Sulfate and Pyrite Series. It can be seen that, besides the C_2-C_5 gases, methane is also consumed in the $MgSO_4$ series accompanied by larger yields in CO_2 compared to the control series (Figure 4a–c, e). Therefore, it is likely that the C_1-C_5 was directly oxidized by strong $MgSO_4$ TSR, which can be explained by the reduction of bisulfate ions (HSO_4^-) and aqueous magnesium sulfate contact ion pairs ($[MgSO_4]_{CIP}$) at low pH values.[9,11,28] The effect of $CaSO_4$ on gas yields and isotopic compositions is much milder than in the $MgSO_4$ series. Nevertheless, lower yields of hydrocarbons and less negative ^{13}C isotope values than in the control series can be observed.

In the pyrite series, maximum yields of gaseous and liquid compounds are lower and occur at lower temperatures than in the control series. Meanwhile, the methane yields increase at a lower rate when temperatures exceed 432 °C (see section 3.1.1). This indicates that the main influence on methane generation by pyrite is an indirect one through reduction reactions mainly involving wet gases at temperatures exceeding 432 °C, as shown by the decrease in C_{2-5} yields and the enrichment of ^{13}C in ethane >432 °C and propane >408 °C (Figure 6b and c). Generally, the overall effect of pyrite on gaseous hydrocarbon generation is much milder than that of sulfates. Due to the impact of pyrite and sulfates on the hydrocarbon gas yields, it can be deduced that (1) low concentrations of C_1-C_5 and high amounts of H_2S will be expected in sulfate-rich environments and (2) higher H_2S yields will occur under high thermal pressure when pyrite is widely present.

4.3. Reaction Mechanisms in the Pyrite and Sulfate Series. For a better understanding of the effect of inorganically bound sulfur on gas compositions and $\delta^{13}C$ values at high temperatures, we provide the relationship between the CO_2 and H_2S yields through our experiments. Generally, there is a linear relationship between CO_2 and H_2S yields in sulfates and pyrite treatments, which is shown in Figure 7. The fitted linear equations (dotted straight lines) can be expressed as the following.

For $MgSO_4$:

$$y = 1.463x + 262.4;\ R^2 = 0.963 \quad (1)$$

For pyrite:

$$y = 0.197x + 17.24;\quad R^2 = 0.939 \quad (2)$$

dx.doi.org/10.1021/ef401468w | *Energy Fuels* 2014, 28, 785−793

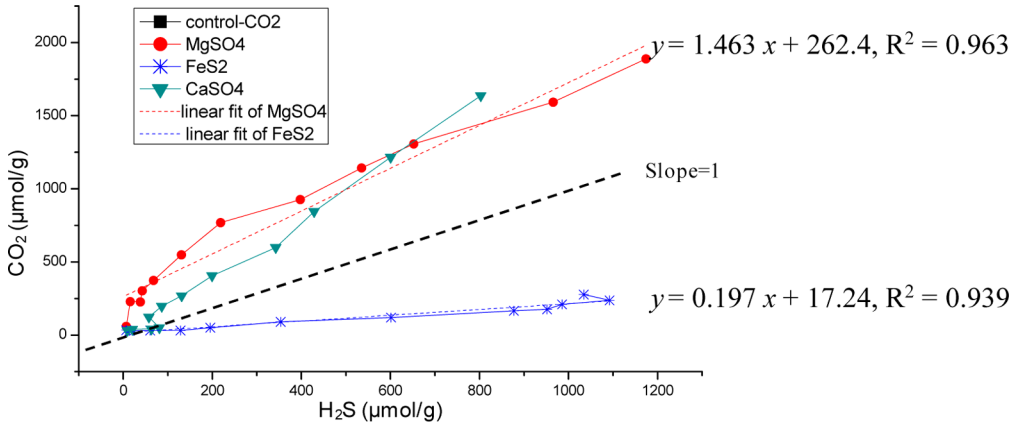

Figure 7. CO_2 concentration versus H_2S concentration with linear fits (dotted lines).

where y is CO_2 yield and x is H_2S yield in μmole per g of shale sample. The slopes, equivalent to the CO_2/H_2S ratios, are 1.463 and 0.197 for $MgSO_4$ and pyrite, respectively.

There is no doubt that TSR occurs in the sulfate environments, affecting the organic and inorganic gas yields and their isotopic values. However, the mechanism of pyrite affecting the gaseous hydrocarbon yields is not clear. Based on literature, the reaction of sulfur in different valences with hydrocarbons can be generalized as follows:[5,9,13,23,28]

$$SO_4^{2-} + 1.33(CH_2) + 0.66H_2O \rightarrow H_2S + 1.33CO_2 + 2OH^- \quad (3)$$

$$4S^0 + 1.33(CH_2) + 2.66H_2O \rightarrow 4H_2S + 1.33CO_2 \quad (4)$$

It should be noted that S^0 in eq 4 stands for elemental sulfur or other intermediate oxidation states of sulfur with lower valences than SO_4^{2-}, that is, <+6, such as polysulfides.[5,23] The theoretical ratio of CO_2/H_2S in TSR shown in eq 3 is 1.33:1, consistent with the slope (1.463; >1) of our fitting eq 1. Similarly, the slope (0.197; <1) of the pyrite series in eq 2 is closer to the theoretical ratio of CO_2/H_2S in eq 4, indicating that the reaction between pyrite and hydrocarbons mainly proceeds through S^0.

4.4. Isotopic Reversal for Ethane. In the control series, the $\delta^{13}C$ values of ethane increase with temperature up to 552 °C and slightly decrease above 552 °C (isotopic reversal, i.e., decrease in $\delta^{13}C$ values with increasing maturity or temperature). A more remarkable isotopic reversal (rollover) is observed in the pyrite series. The sudden drop and then gradual increase in $\delta^{13}C$ value for temperatures exceeding 504 °C are consistent with newly increasing ethane yields in the same temperature range, clearly indicating a new source for ethane with more negative $\delta^{13}C$ values above 504 °C.

Many explanations have been proposed for the isotopic reversal. Jenden et al.[38] ascribed the isotopic reversal in Appalachian Basin shale to the mixing of gases generated under different maturities. Lewan suggested that hydrous wet gas cracking may lead to the isotopic rollover trend.[39] Zumberge et al.[22] used a two-stage reaction scheme to interpret the isotopic reversal in the unconventional Barnett and Fayetteville shale gas systems: (1) H_2 and isotopically light CO_2 were generated by reactions between water and hydrocarbons (methane), and (2) H_2 and CO_2 further react to form light ethane under the catalysis of shale minerals. It seems that water possibly plays a very important role in the reactions with hydrocarbons/kerogen. In our experiments, the possibility of wet gas cracking to light C_2 can be ruled out because extremely low yields in C_{3-5} (0.6−0 μmol/g rock at 480−600 °C in Figure 4c) are insufficient to provide the source for ethane above 504 °C. Thus, we rationalize that organic matter in the form of kerogen/coke/pyrobitumen and water may react with each other to form isotopically light C_2 at high temperatures (>504 °C).

It is worth mentioning that the isotopic reversal in the pyrite series is more obvious than that in the control series. For the former more ethane was consumed resulting in isotopically heavier ethane at very low concentrations at 504 °C. Above 504 °C, new, isotopically light ethane emerged (Figure 6b), causing the reversal phenomenon. In the control series, much higher residual amounts of ethane caused the newly formed, light ethane to be overlooked. Considering that pyrite is very common in North American shales,[18,19] pyrite may cause the isotopic reversal to be more evident in those unconventional shale gas systems.

5. CONCLUSIONS

Simulation experiments of mature shales with added minerals (sulfates and pyrite) have been carried out to investigate the effect of inorganically bound sulfur on gas generation. The yields of organic and inorganic gases and their stable carbon isotopic compositions have been measured. The results provide new insight into the reaction mechanisms between gaseous hydrocarbons and sulfur-containing minerals ($MgSO_4$, $CaSO_4$, and pyrite).

The experimental results for the mature Salgan Shale sample in the control series demonstrate the huge potential for late methane generation, which can be deduced from the maximum methane yield of 593 μmol/g at 600 °C (highest applied experimental temperature). In this sample, the gaseous hydrocarbons can be mainly ascribed to the primary cracking of higher molecular weight (MW) analogues in kerogen rather than the secondary cracking from oil. Degradation of gaseous hydrocarbons in sulfate and pyrite treatments is severe at high temperatures, leading to decreased pyrolysis yields and a heavier carbon isotope signature. Strong TSR occurs very early at already lowest temperatures in $MgSO_4$ treatments while moderate TSR occurs in $CaSO_4$ treatments later, that is, at higher temperatures. Pyrite directly affects wet gas (C_2-C_5) evolution and thus indirectly affects methane evolution while sulfates directly affect C_1-C_5 evolution. Thus, low yields of C_1-C_5 coupled with quantities of H_2S will be expected in sulfate/pyrite-rich environment under high thermal pressure.

dx.doi.org/10.1021/ef401468w | Energy Fuels 2014, 28, 785−793

The difference in CO_2/H_2S ratio evolution with artificial maturity between the pyrite and sulfate series indicates different reaction mechanisms. The yield ratio evolution between CO_2 and H_2S in pyrite treatments can be explained by gas reduction through S^0. A remarkable isotopic reversal and a gradual increase in ethane yield at temperatures exceeding 504 °C indicate a new origin for ethane at high temperatures. In our opinion, the reactions between water and solid carbon entities (kerogen/coke/pyrobitumen) play an important role in forming the new and isotopically light ethane. Our experiments reveal that pyrite content might play an important role for the occurrence of isotopic rollovers in natural shale gas systems. The composition of shale gas that is locked in the rock and released/recovered by hydraulic fracturing might therefore depend on the mineralogical composition influenced by the depositional environment and thermal stress through tectonic movement over geological time. Our studies might provide some leads to the prediction of gas composition based on the mineral contents.

■ ASSOCIATED CONTENT

Supporting Information

Additional data in an Excel document. This material is available free of charge via the Internet at http://pubs.acs.org.

■ AUTHOR INFORMATION

Corresponding Authors

*Tel.: +86 20 85290191. E-mail: luhong@gig.ac.cn.
*Tel.: 860-410-6684. E-mail: chsu@fsu.edu.

Notes

The authors declare no competing financial interest.

■ ACKNOWLEDGMENTS

The authors are indebted to the reviewer for his insightful comments and suggestions, which significantly improves the manuscript. We also thank Dr. Zou Yanrong and Dr. Pan Changchun for their useful suggestions for the revision of the paper. Financial support for this work was gratefully received from State 973 project (2012CB214706), major national science and technology projects (2011ZX05008-002-33), and NSFC project (40873048, 41173053). This is contribution No. IS-1817 from GIG CAS.

■ REFERENCES

(1) Tissot, B. P.; Welte, D. H. *Petroleum Formation and Occurrence*; Springer Verlag: Berlin, 1984.
(2) Wang, F.; He, Z.; Meng, X.; Bao, L.; Zhang, H. Occurrence of shale gas and prediction of original gas in place (OGIP). *Nat. Gas Geosci.* **2011**, *22*, 501−510.
(3) Erdmann, M.; Horsfield, B. Enhanced late gas generation potential of petroleum source rocks via recombination reactions: Evidence from the Norwegian North Sea. *Geochim. Cosmochim. Acta* **2006**, *70*, 3943−3956.
(4) Mahlstedt, N.; Horsfield, B. Metagenetic methane generation in gas shales I. Screening protocols using immature samples. *Mar. Petrol. Geol.* **2012**, *31*, 27−42.
(5) Orr, W. L. Changes in sulfur content and isotopic ratios of sulfur during petroleum maturation; study of Big Horn basin Paleozoic oils. *AAPG Bull.* **1974**, *58*, 2295−2318.
(6) Krouse, H. R.; Viau, C. A.; Eliuk, L. S.; Ueda, A.; Halas, S. Chemical and isotopic evidence of thermochemical sulphate reduction by light hydrocarbon gases in deep carbonate reservoirs. *Nature* **1988**, *333*, 415−419.
(7) Cross, M. M.; Manning, D. A. C.; Bottrell, S. H.; Worden, R. H. Thermochemical sulphate reduction (TSR): Experimental determination of reaction kinetics and implications of the observed reaction rates for petroleum reservoirs. *Org. Geochem.* **2004**, *35*, 393−404.
(8) Cai, C.; Xie, Z.; Worden, R. H.; Hu, G.; Wang, L.; He, H. Methane-dominated thermochemical sulphate reduction in the Triassic Feixianguan Formation East Sichuan Basin, China: Towards prediction of fatal H_2S concentrations. *Mar. Petrol. Geol.* **2004**, *21*, 1265−1279.
(9) Ma, Q.; Ellis, G. S.; Amrani, A.; Zhang, T.; Tang, Y. Theoretical study on the reactivity of sulfate species with hydrocarbons. *Geochim. Cosmochim. Acta* **2008**, *72*, 4565−4576.
(10) Zhang, T.; Ellis, G. S.; Walters, C. C.; Kelemen, S. R.; Wang, K.; Tang, Y. Geochemical signatures of thermochemical sulfate reduction in controlled hydrous pyrolysis experiments. *Org. Geochem.* **2008**, *39*, 308−328.
(11) Lu, H.; Greenwood, P.; Chen, T.; Liu, J.; Peng, P.a. The role of metal sulfates in thermochemical sulfate reduction (TSR) of hydrocarbons: Insight from the yields and stable carbon isotopes of gas products. *Org. Geochem.* **2011**, *42*, 700−706.
(12) Worden, R. H.; Smalley, P. C.; Barclay, S. A. H_2S and diagenetic pyrite in North Sea sandstones: Due to TSR or organic sulphur compound cracking? *J. Geochem. Explor.* **2003**, *78*−*79*, 487−491.
(13) Amrani, A.; Zhang, T.; Ma, Q.; Ellis, G. S.; Tang, Y. The role of labile sulfur compounds in thermochemical sulfate reduction. *Geochim. Cosmochim. Acta* **2008**, *72*, 2960−2972.
(14) Heydari, E. The role of burial diagenesis in hydrocarbon destruction and H_2S accumulation, Upper Jurassic Smackover Formation, Black Creek Field, Mississippi. *AAPG Bull.* **1997**, *81*, 26−45.
(15) Sassen, R. Geochemical and carbon isotopic studies of crude oil destruction, bitumen precipitation, and sulfate reduction in the deep Smackover Formation. *Org. Geochem.* **1988**, *12*, 351−361.
(16) Machel, H. G. Bacterial and thermochemical sulfate reduction in diagenetic settings—Old and new insights. *Sediment. Geol.* **2001**, *140*, 143−175.
(17) Mello, M.; Telnaes, N.; Maxwell, J. The hydrocarbon source potential in the Brazilian marginal basins: A geochemical and paleoenvironmental assessment. In *Paleogeography, Paleoclimate, and Source Rocks*; Huc, A. Y., Ed.; American Association of Petroleum Geologists: Tulsa, 1995: Vol. *40*, pp 233−272.
(18) Martini, A. M.; Walter, L. M.; Ku, T. C. W.; Budai, J. M.; McIntosh, J. C.; Schoell, M. Microbial production and modification of gases in sedimentary basins: A geochemical case study from a Devonian shale gas play, Michigan basin. *AAPG Bull.* **2003**, *87*, 1355−1375.
(19) Loucks, R. G.; Ruppel, S. C. Mississippian Barnett Shale: Lithofacies and depositional setting of a deep-water shale-gas succession in the Fort Worth Basin, Texas. *AAPG Bull.* **2007**, *91*, 579−601.
(20) Metecan, İ.H.; Sağlam, M.; Yanık, J.; Ballice, L.; Yüksel, M. The effect of pyrite catalyst on the hydroliquefaction of Göynük (Turkey) oil shale in the presence of toluene. *Fuel* **1999**, *78*, 619−622.
(21) Chalmers, G. R. L.; Bustin, R. M. Geological evaluation of Halfway−Doig−Montney hybrid gas shale−tight gas reservoir, northeastern British Columbia. *Mar. Petrol. Geol.* **2012**, *38*, 53−72.
(22) Zumberge, J.; Ferworn, K.; Brown, S. Isotopic reversal ('rollover') in shale gases produced from the Mississippian Barnett and Fayetteville formations. *Mar. Petrol. Geol.* **2012**, *31*, 43−52.
(23) Seewald, J. S. Organic−inorganic interactions in petroleum-producing sedimentary basins. *Nature* **2003**, *426*, 327−333.
(24) Chen, X.; Zhang, Y.; Li, Y.; Fan, J.; Tang, P.; Chen, Q.; Zhang, Y. Biostratigraphic correlation of the Ordovician black shales in Tarim Basin and its peripheral regions. *Science China Earth Sciences* **2012**, *55*, 1230−1237.
(25) Xiao, X.; Wilkins, R. W. T.; Liu, D.; Liu, Z.; Fu, J. Investigation of thermal maturity of lower Palaeozoic hydrocarbon source rocks by means of vitrinite-like maceral reflectance—A Tarim Basin case study. *Org. Geochem.* **2000**, *31*, 1041−1052.
(26) Wang, F.; He, P.; Cheng, D.; Hao, S.; Liu, D. Take vitrinite-like reflectance as the maturity indicator for lower paleozoic high-over mature source rock. *Nat. Gas Ind.* **1996**, *16*, 14−18.
(27) Pan, C.; Geng, A.; Zhong, N.; Liu, J.; Yu, L. Kerogen pyrolysis in the presence and absence of water and minerals. 1. Gas components. *Energy Fuels* **2008**, *22*, 416−427.

(28) Zhang, T.; Amrani, A.; Ellis, G. S.; Ma, Q.; Tang, Y. Experimental investigation on thermochemical sulfate reduction by H_2S initiation. *Geochim. Cosmochim. Acta* **2008**, *72*, 3518−3530.
(29) Pan, C.; Yu, L.; Liu, J.; Fu, J. Chemical and carbon isotopic fractionations of gaseous hydrocarbons during abiogenic oxidation. *Earth. Planet. Sc. Lett* **2006**, *246*, 70−89.
(30) Behar, F.; Kressmann, S.; Rudkiewicz, J. L.; Vandenbroucke, M. Experimental simulation in a confined system and kinetic modelling of kerogen and oil cracking. *Org. Geochem.* **1992**, *19*, 173−189.
(31) Wang, Q.; Lu, H.; Greenwood, P.; Shen, C.; Liu, J.; Peng, P.a. Gas evolution during kerogen pyrolysis of Estonian Kukersite shale in confined gold tube system. *Org. Geochem.* **2013**, *65*, 74−82.
(32) Machel, H. G.; Krouse, H. R.; Sassen, R. Products and distinguishing criteria of bacterial and thermochemical sulfate reduction. *Appl. Geochem.* **1995**, *10*, 373−389.
(33) Galimov, E. M. Isotope organic geochemistry. *Org. Geochem.* **2006**, *37*, 1200−1262.
(34) Worden, R. H.; Smalley, P. C. H_2S-producing reactions in deep carbonate gas reservoirs: Khuff Formation, Abu Dhabi. *Chem. Geol.* **1996**, *133*, 157−171.
(35) Worden, R. H.; Smalley, P. C.; Oxtoby, N. H. Gas souring by thermochemical sulfate reduction at 140°C. *AAPG Bull.* **1995**, *79*, 854−863.
(36) Cai, C.; Worden, R. H.; Bottrell, S. H.; Wang, L.; Yang, C. Thermochemical sulphate reduction and the generation of hydrogen sulphide and thiols (mercaptans) in Triassic carbonate reservoirs from the Sichuan Basin, China. *Chem. Geol.* **2003**, *202*, 39−57.
(37) Lorant, F.; Prinzhofer, A.; Behar, F.; Huc, A. Y. Carbon isotopic and molecular constraints on the formation and the expulsion of thermogenic hydrocarbon gases. *Chem. Geol.* **1998**, *147*, 249−264.
(38) Jenden, P.; Drazan, D.; Kaplan, I. Mixing of thermogenic natural gases in northern Appalachian Basin. *AAPG Bull.* **1993**, *77*, 980−998.
(39) Lewan, M. D. Experiments on the role of water in petroleum formation. *Geochim. Cosmochim. Acta* **1997**, *61*, 3691−3723.